# Effects of defect states on the performance of $CuInGaSe_2$ solar cells*

Wan Fucheng(万福成)[1], Tang Fuling(汤富领)[1,2,†], Xue Hongtao(薛红涛)[1], Lu Wenjiang(路文江)[1,2], Feng Yudong(冯煜东)[2], and Rui Zhiyuan(芮执元)[1]

[1]State Key Laboratory of Gansu Advanced Non-ferrous Metal Materials, Department of Materials Science and Engineering, Lanzhou University of Technology, Lanzhou 730050, China
[2]Science and Technology on Surface Engineering Laboratory, Lanzhou Institute of Physics, Lanzhou 730000, China

**Abstract:** Device modeling has been carried out to investigate the effects of defect states on the performance of ideal $CuInGaSe_2$ (CIGS) thin film solar cells theoretically. The varieties of defect states (location in the band gap and densities) in absorption layer CIGS and in buffer layer CdS were examined. The performance parameters: open-circuit voltage, short-circuit current, fill factor, and photoelectric conversion efficiency for different defect states were quantitatively analyzed. We found that defect states always harm the performance of CIGS solar cells, but when defect state density is less than $10^{14}$ $cm^{-3}$ in CIGS or less than $10^{18}$ $cm^{-3}$ in CdS, defect states have little effect on the performances. When defect states are located in the middle of the band gap, they are more harmful. The effects of temperature and thickness are also considered. We found that CIGS solar cells have optimal performance at about 170 K and 2 $\mu$m of CIGS is enough for solar light absorption.

**Key words:** device modeling; defect states; solar cell; conversion efficiency
**DOI:** 10.1088/1674-4926/35/2/024011 **PACC:** 8630J; 7155E; 7125R

## 1. Introduction

As one of the most promising photovoltaic materials, I–III–$VI_2$ ternary chalcopyrites, such as $Cu(In_{1-x}Ga_x)Se_2$ (CIGS), has high photoelectric conversion efficiency (20.3%) and can be used in thin film solar cells[1−5]. The CIGS-based solar cells also exhibit excellent outdoor stability on the earth and radiation hardness for use in outer space[6−8]. In order to improve the overall performance of CIGS cells, increasing the open-circuit voltage ($V_{oc}$) and the short-circuit current density ($J_{sc}$) is highly desirable because this minimizes the interconnection losses in the manufacture of cell modules[3]. However, unavoidable defect states emerge in solar cell materials, introduced by void, doping, surface or interface, which always decrease $V_{oc}$ and $J_{sc}$ then deteriorate the cell's performance[9−11]. For example, the band gap of the CIGS absorber is engineered by doping Ga. The anticipated changes in the physical properties of the $CuInSe_2$ (CIS) films with the addition of Ga include an increase in band gap, which mainly shifts the position of the conduction-band minimum[12], as well as changes in the hole concentration[13], bulk defect densities[14], absorption coefficients, and electron affinities. Some of these changes have also been confirmed by our previous works from first principles[15−18]. Hinuma *et al.*[19] obtained the valence band offsets of the CIS/CdS and CIS/ZnS (110) interfaces using first-principles calculations. They also found that there are no clear interface states in the CIS region, but in the CdS region there are interface states composed mainly of S3p orbitals at two layers from the interface between about –1 to 0 eV from the highest occupied state in the interface supercell. Defect states in the band gap of the absorption material or buffer layer material produces discrete $V_{oc}$ values for different solar cells. Dharmadasa *et al.*[20] found that there are four possible defect states in CIGS solar cells, four potential barriers, and hence four groups of $V_{oc}$ values can be expected. This phenomenon has been experimentally observed and been identified separately for good devices with high efficiencies (> 12%)[21−25]. In this paper, device modeling and numerical simulations of CIGS cells are performed to analyze the impacts of defect states in the CIGS absorption layers and those in the CdS buffer layer on the performance parameters of the solar cells[26]. Such modeling will provide an insight into how defect states affect a cell's performance. The investigation focuses on the study of the effects on performance caused by various defect states (location in the band gap and their state densities). Additionally, the effects of work temperature and thickness of CIGS and CdS are also simulated[27]. Based on the simulation results, an optimal work temperature and the economical band and geometrical structure for the CIGS cell is proposed.

## 2. Methodology

The modeling calculations performed in the following section use the AMPS-1D software (analysis of microelectronic and photonic structures)[28]. This method estimates the steady-state band diagram, recombination profile, carrier transport in one dimension based on the Poisson equation, and the hole and electron continuity equations. They are given respectively by Eqs. (1) to (3)[8]:

* Project supported by the National Natural Science Foundation of China (Nos. 11164014, 11364025, 51065014) and the Science and Technology Pillar Program of Gansu Province (No. 1204GKCA057).
† Corresponding author. Email: tfl03@mails.tsinghua.edu.cn
Received 13 July 2013, revised manuscript received 14 August 2013

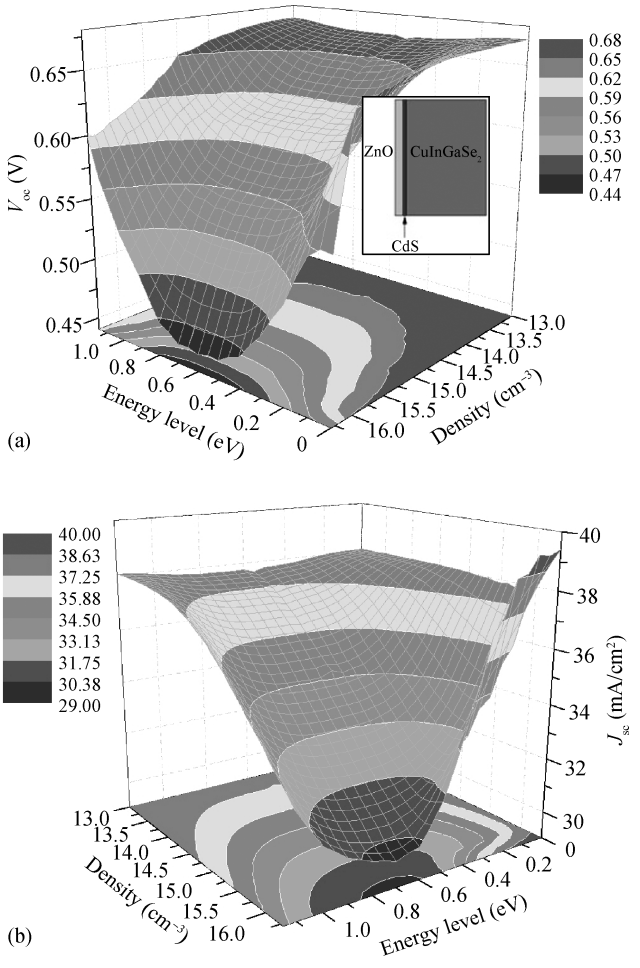


Fig. 1. The variation of the (a) open-circuit voltage ($V_{oc}$) and (b) short-circuit current ($J_{sc}$) with defect state in CIGS. Inset of (a) is the structural model of a CIGS solar cell.

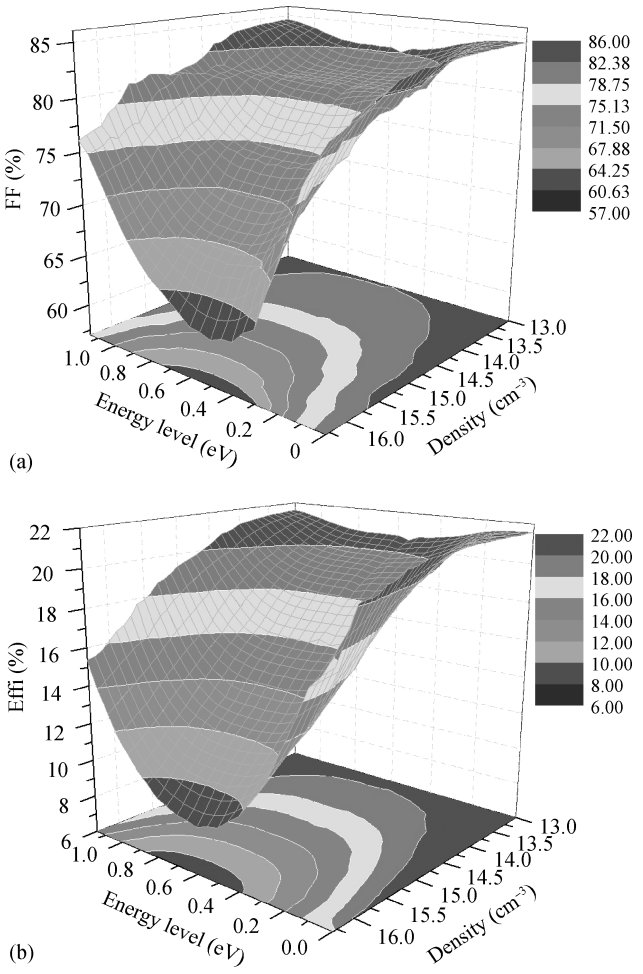


Fig. 2. The change of the (a) fill factor (FF) and (b) photoelectric conversion efficiency (Effi) with defect state in CIGS.

$$\frac{\mathrm{d}}{\mathrm{d}x}\left(-\varepsilon(x)\frac{\mathrm{d}\psi}{\mathrm{d}x}\right) = q\left[p(x) - n(x) + N_{\mathrm{d}}^{+}(x) - N_{\mathrm{A}}^{-}(x) + p_{\mathrm{t}}(x) - n_{\mathrm{t}}(x)\right], \tag{1}$$

$$\frac{\mathrm{d}p_{\mathrm{n}}}{\mathrm{d}t} = G_{\mathrm{p}} - \frac{p_{\mathrm{n}} - p_{\mathrm{n0}}}{\tau_{\mathrm{p}}} - p_{\mathrm{n}}\mu_{\mathrm{p}}\frac{\mathrm{d}\xi}{\mathrm{d}x} - \mu_{\mathrm{p}}\xi\frac{\mathrm{d}p_{\mathrm{n}}}{\mathrm{d}x} + D_{\mathrm{p}}\frac{\mathrm{d}^2p_{\mathrm{n}}}{\mathrm{d}x^2}, \tag{2}$$

$$\frac{\mathrm{d}n_{\mathrm{p}}}{\mathrm{d}t} = G_{\mathrm{n}} - \frac{n_{\mathrm{p}} - n_{\mathrm{p0}}}{\tau_{\mathrm{n}}} + n_{\mathrm{p}}\mu_{\mathrm{n}}\frac{\mathrm{d}\xi}{\mathrm{d}x} + \mu_{\mathrm{n}}\xi\frac{\mathrm{d}n_{\mathrm{p}}}{\mathrm{d}x} + D_{\mathrm{n}}\frac{\mathrm{d}^2n_{\mathrm{p}}}{\mathrm{d}x^2}, \tag{3}$$

where $\Psi$ is the electrostatic potential and $p$ the free hole, $n$ the free electron, $p_{\mathrm{t}}$ the trapped hole, $n_{\mathrm{t}}$ the trapped electron, $N_{\mathrm{A}}^{-}$ the ionized acceptor-like doping and $N_{\mathrm{d}}^{+}$ the ionized donor-like doping concentrations, and $\xi$ the electric field. All of the above parameters are functions of the coordinate position $x$ in the CIGS solar cells. $p_{\mathrm{n}}$ (holes) and $n_{\mathrm{p}}$ (electrons) are the minority carrier densities in n-type and p-type materials, respectively, $G$ is the carrier generation rate, $\tau$ the carrier lifetime, $\mu$ the carrier mobility, $\varepsilon$ the permittivity, $D$ the carrier diffusion coefficient, and $q$ the electron charge. Recombination currents are calculated with the Shockley–Read–Hall (SRH) model for bulk defects and an extension of the SRH model for interface defects. The SRH interface approach allows carriers from both conduction and valence bands to participate in the interface recombination process.

In this device simulation, we have considered an ideal and simple CIGS cell (the cell structure is shown in the inset of Fig. 1(a)) structure with following material layers: 0.2 $\mu$m ZnO, 0.05 $\mu$m CdS, and 3 $\mu$m CIGS. The most widely assumed concept is the hetero-junction formed between a p-type CIGS material and an n-type CdS layer. Up to now, most of the research and analysis carried out are based on this hetero-junction concept. In the simulation, an electron mobility $\mu_{\mathrm{n}} = 10\ \mathrm{cm}^2/(\mathrm{V{\cdot}s})$, a carrier density $n = 10^{12}\ \mathrm{cm}^{-3}$, and a band-gap $E_{\mathrm{g}} = 1.15$ eV have been used for the absorber $CuIn_{1-x}Ga_xSe_2$. Semiconductor parameters of each layer of the cell structure were inputted into AMPS-1D simulation software. In the software, NREL 1.5 spectral intensity as a function of wavelength is used[29].

## 3. Results and discussion

### 3.1. Effects of defect states in $CuInGaSe_2$

Effects of a donor defect state in $CuInGaSe_2$ are shown in Figs. 1 and 2. The location of the defect state is theoretically changed from the bottom of the conductivity band to the top of the valance band. At the same time, the defect state is idealized from $1.0 \times 10^{13}$ to $2.0 \times 10^{16}\ \mathrm{cm}^{-3}$. The energy level of the defect state is a positive value down from the bottom of the

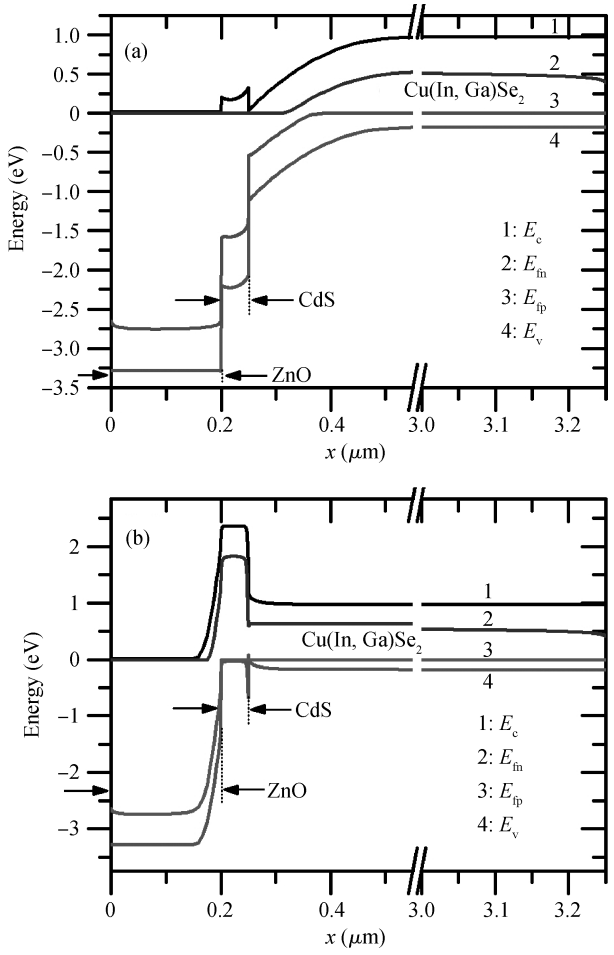


Fig. 3. Band structure of a CIGS solar cell with (a) low defect density and (b) high defect density in CdS.

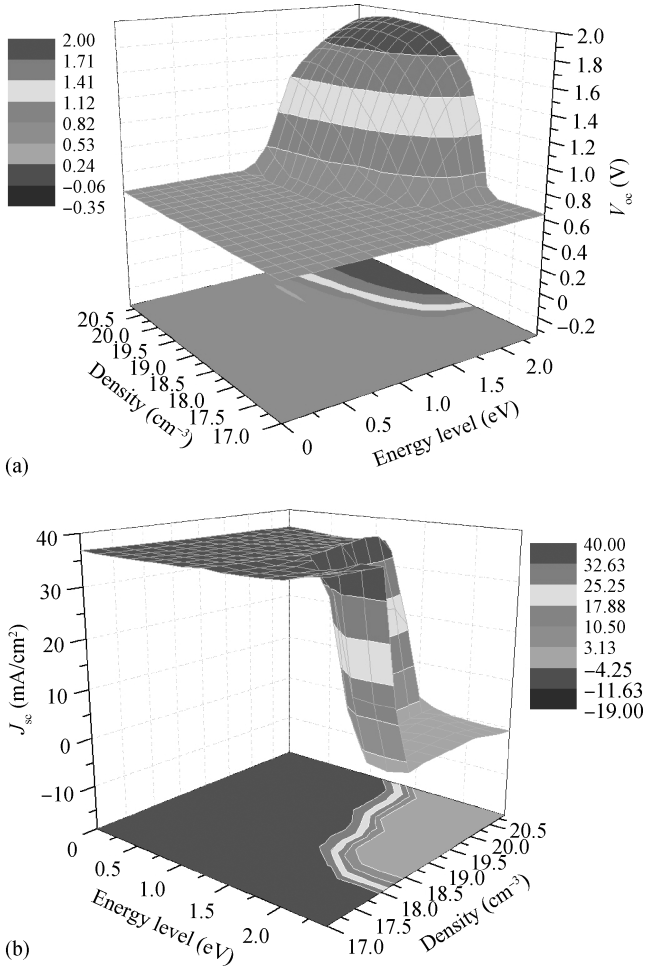


Fig. 4. The variation of the open-circuit voltage ($V_{oc}$) and short-circuit current ($J_{sc}$) with the location and the density of the defect state in CdS.

conductivity band (the band gap of CIGS is set as 1.15 eV). The change of open-circuit voltage $V_{oc}$ is shown in Fig. 1(a). When the defect state is less than $5.5 \times 10^{13}$ cm$^{-3}$, $V_{oc}$ changes slightly around 0.67 V, while the location of the defect state has little effect. As the defect state is larger than $5.5 \times 10^{13}$ cm$^{-3}$, $V_{oc}$ is sensitive to the change of defect state density, especially to the change of the location of defect state. When the defect state is about $2 \times 10^{16}$ cm$^{-3}$, $V_{oc}$ decreases to 0.45 V with a middle location of defect state in the band gap. In Fig. 1(a), when the defect state is larger than $10^{15}$ cm$^{-3}$, $V_{oc}$ with a defect state located at the bottom of conductivity band is larger than the $V_{oc}$ with a defect state located on the top of the valence band.

The change of short-circuit current $J_{sc}$ (Fig. 1(b)) is similar to that of $V_{oc}$. When the defect state is less than $3 \times 10^{13}$ cm$^{-3}$, $J_{sc}$ changes slightly around 38 mA/cm$^2$; here $J_{sc}$ is not sensitive to the location of the defect state. As the defect state is larger than $3 \times 10^{13}$ cm$^{-3}$, $J_{sc}$ is sensitive to the change of defect state density, especially to the change of the location of defect state. When the defect state is about $1.5 \times 10^{16}$ cm$^{-3}$, $J_{sc}$ decreases to 30 mA/cm$^2$ with a middle location of defect state in the band gap. However, we also note that even the defect state is larger than $10^{16}$ cm$^{-3}$, but the defect state is located at the bottom of the conductivity band, $J_{sc}$ has its maximum value of 39 mA/cm$^2$.

The change of fill factor FF and photoelectric conversion efficiency Effi are shown in Figs. 2(a) and 2(b), respectively. They are sensitive to the change of both of the location and the density of defect states. As the defect state increases from $1.0 \times 10^{13}$ to $2.0 \times 10^{16}$ cm$^{-3}$ and as the defect state approaches to the middle of the gap, FF decreases from 86% to 60%, while Effi decreases from 22% to 8.5%. Defect states on the top of the valence band have a larger disadvantageous effect on the overall performance of CIGS solar cells than that at the bottom of conductivity band. The band structure of the solar cell is illustrated in Fig. 3(a), and $V_{oc}$ can be obtained as $E_{fn} - E_{fp}$.

### 3.2. Effects of defect states in CdS

The effects of an accepter defect state in CdS are shown in Figs. 4 and 5. The location of the defect state is theoretically changed from the bottom of conductivity band to the top the bottom of the valance band. Meanwhile, the defect state is idealized from $1.0 \times 10^{17}$ to $8.0 \times 10^{20}$ cm$^{-3}$. The change of open-circuit voltage $V_{oc}$ is shown in Fig. 4(a). The energy level of the defect state is a positive value down from the bottom of the conductivity band (the band gap of CdS is set as 2.4 eV). We note that defect states in CdS always have little effect on $V_{oc}$ (it keeps stable about 0.64 V), except when the

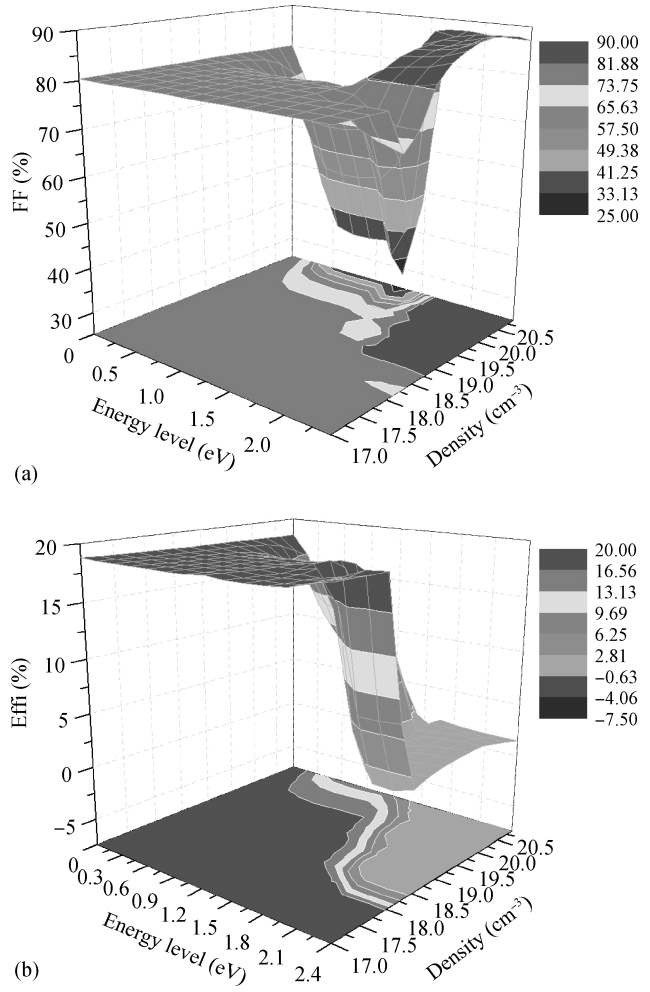


Fig. 5. The change of the fill factor (FF) and photoelectric conversion efficiency (Effi) with the location and the density of the defect state in CdS.

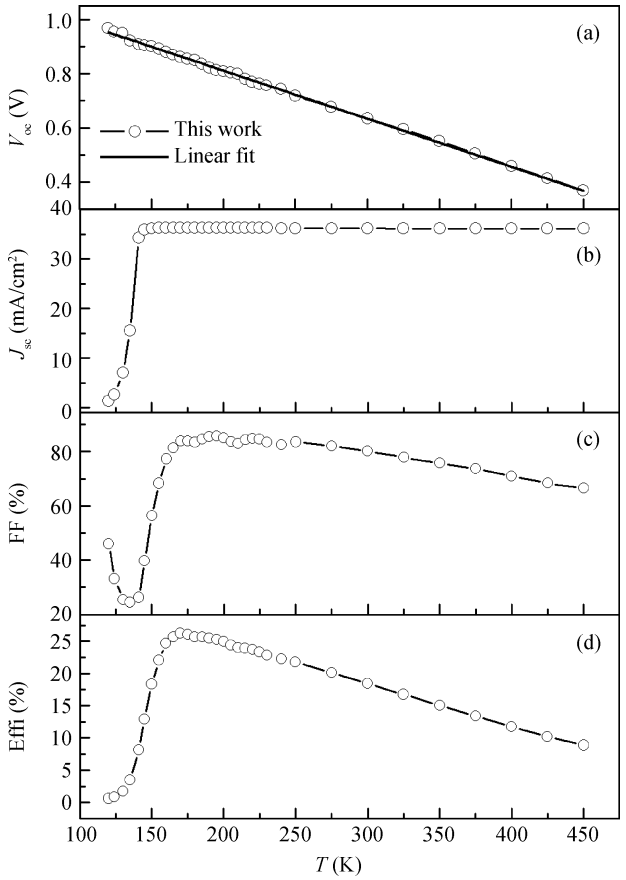


Fig. 6. The dependence of the open-circuit voltage ($V_{oc}$), short-circuit current ($J_{sc}$), fill factor (FF), and photoelectric conversion efficiency (Effi) with temperature.

defect state approaches the top of valence band and its density is larger than $1.3 \times 10^{18}$ cm$^{-3}$ ($V_{oc}$ increases gradually up to 1.94 V). The reason why can be seen in Fig. 3(b): the forbidden band of CdS is located above the forbidden band of CIGS, and the built-in electric field in the p–n junction has the opposite direction compared with the normal p–n junction in Fig. 3(a). The change of short-circuit current $J_{sc}$ is shown in Fig. 4(b). We also note that defect states in CdS always have little effect on $J_{sc}$ (it keeps stable about 36 mA/cm$^2$), except when the defect state approaches the top of valence band and its density is larger than $8 \times 10^{17}$ cm$^{-3}$ (contrary to that of $V_{oc}$ in Fig. 1(a), $J_{sc}$ decreases sharply to 0 mA/cm$^2$).

The change of fill-factor FF and photoelectric conversion efficiency Effi is shown in Figs. 5(a) and 5(b), respectively. Generally, they are not sensitive to the change of the location when the density of defect states is less than $5.5 \times 10^{18}$ cm$^{-3}$. As the defect state increases up to $5.0 \times 10^{20}$ cm$^{-3}$ and as the defect state approaches to the middle of the gap, FF decreases from 86% to 30%. When defect state increases up to about $6 \times 10^{18}$ cm$^{-3}$ and as the defect state approaches the top of the valence band it increases to its maximum value of 85%. When the defect state locates on the top of the valence band and its value ranges from $1.0 \times 10^{18}$ to $3.0 \times 10^{18}$ cm$^{-3}$, it has a local minimum value of about 71.6%. As the defect state increases from $1.0 \times 10^{18}$ to $3.2 \times 10^{18}$ cm$^{-3}$ and as the defect state approaches the top of the valence band, Effi decreases sharply from 20% to almost zero. All in all, defect states in CdS have smaller effects than those in CIGS.

### 3.3. Effects of temperature and thickness

Effects of temperature are shown in Fig. 6. As temperature ($T$) increases from 120 to 450 K, $V_{oc}$ decreases linearly from about 0.97 to 0.37 V: $V_{oc}$ (V) $= -0.00177T$ (K) $+ 1.16598$ (Fig. 6(a)). As $T$ increases from 120 to 145 K, $J_{sc}$ sharply increases from 1.4 to 36 mA/cm$^2$ and keeps almost unchangeable until $T = 450$ K. FF decreases to the minimum 24.4% as $T$ increases from 120 to 135 K, then increases sharply to the maximum 85.7% as $T$ increases from 135 to about 195 K then decreases until $T = 450$ K. Effi increases slightly from 0.6% to 3.5% as $T$ increases from 120 to 135 K, then increases sharply to the maximum 26.2% as $T$ increases from 135 to about 170 K then decreases until $T = 450$ K. Our results indicate that CIGS thin film solar cells have the best performance at the temperature of about 170 K.

Effects of thickness in absorption layer CIGS or that of buffer layer CdS are shown in Figs. 7 and 8. As the thickness of CIGS increases from 0.5 to 2 $\mu$m, $V_{oc}$ increases from 0.61 to 0.63 V. When the thickness of CIGS increases from 2 to 5 $\mu$m, $V_{oc}$ increases slowly from 0.630 to 0.635 V (if the thickness of

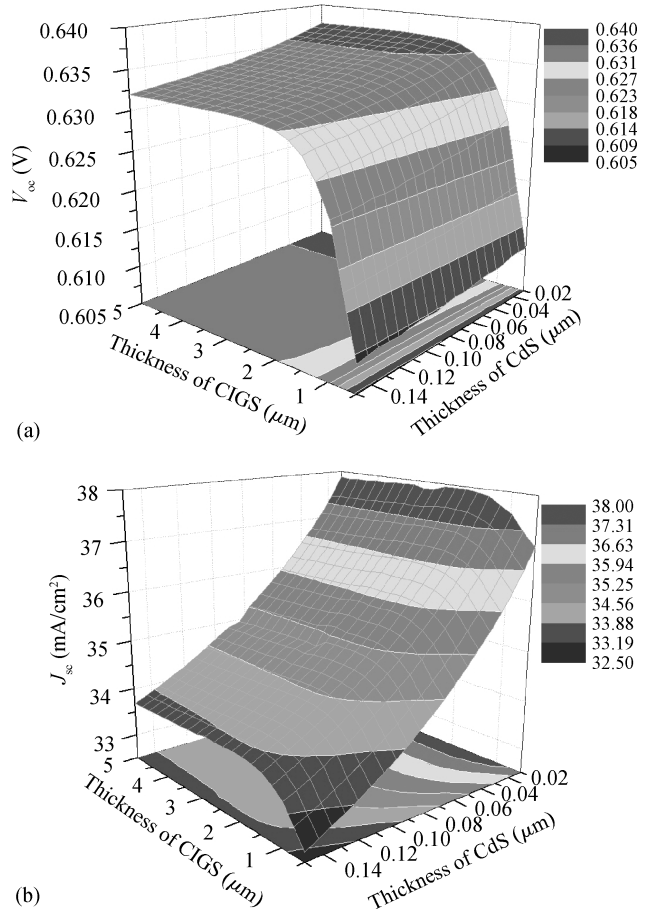


Fig. 7. The variation of the open-circuit voltage ($V_{oc}$) and short-circuit current ($J_{sc}$) with the thickness of CIGS and CdS layers.

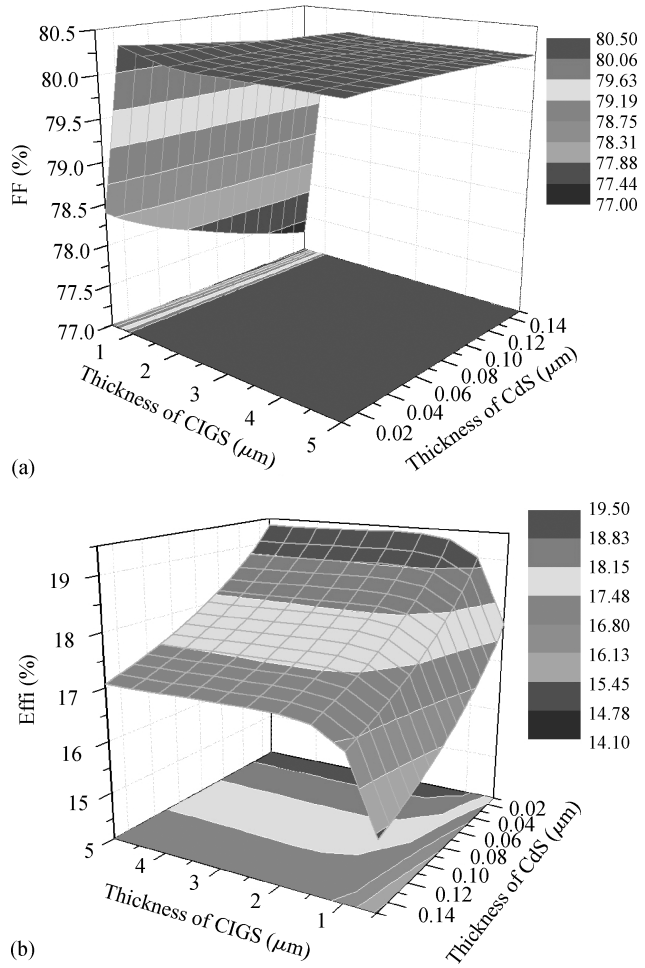


Fig. 8. The change of the fill factor (FF) and photoelectric conversion efficiency (Effi) with the thickness of CIGS and CdS layers.

CdS is 0.05 $\mu$m). Contrary to what we see in CIGS, the thickness of CdS has a negative but very small effect on $V_{oc}$: as it increases from 0.01 to 0.15 $\mu$m $V_{oc}$ decreases about 0.005 V (Fig. 7(a)). Thicknesses of CIGS and CdS have slightly larger effects on $J_{sc}$ that those on $V_{oc}$. As the thickness of CIGS increases from 0.5 to 2 $\mu$m, $J_{sc}$ increases sharply from 35.3 to 36.3 mA/cm$^2$ (if the thickness of CdS is 0.05 $\mu$m, Fig. 7(b)). When the thickness of CIGS increases from 2 to 5 $\mu$m, $J_{sc}$ keeps almost stable. Also contrary to what we see in CIGS, the thickness of CdS has a negative and larger effect on $J_{sc}$: as it increases from 0.02 to 0.14 $\mu$m $J_{sc}$ decreases by about 3.5 mA/cm$^2$.

Thicknesses of CIGS and CdS have similar results on FF, but FF has maximum values when the thickness of CIGS is 1 $\mu$m (Fig. 8(a)). Effi has the same change as that of $J_{sc}$: as the thickness of CIGS increases from 0.5 to 2 $\mu$m, $J_{sc}$ increases sharply from 16.7% to 18.42% (Fig. 8(b), if the thickness of CdS is 0.05 $\mu$m). When the thickness of CIGS increases from 2 to 5 $\mu$m, $J_{sc}$ keeps almost stable. Our results indicate that a 2 $\mu$m thick layer of CIGS is enough for this type of solar cell, a thicker absorption layer will not improve its performance significantly. For the buffer layer CdS (if the preparation condition permits), the thinner the thickness, the better the performance.

## 4. Conclusion

We theoretically performed device modeling on an ideal $CuInGaSe_2$ thin film solar cell to investigate the effects of defect (location in the band gap and densities in absorption layer CIGS and that in buffer layer CdS) states in detail. The open-circuit voltage, short-circuit current, fill factor, and photoelectric conversion efficiency for different defect states were simulated. The effects of temperature and thickness are also simulated. The main results are: (1) the defect states always harm the performance of CIGS solar cells, but when defect state density is less than $10^{14}$ cm$^{-3}$ in CIGS or when it is less than $10^{18}$ cm$^{-3}$ in CdS, defect states have little effect on performance; (2) when defect states are located in the middle of the band gap of CIGS, they are more harmful; (3) CIGS solar cells have optimal performance at about 170 K and 2 $\mu$m of CIGS is enough for solar light absorption; (4) the relationship between open-circuit voltage $V_{oc}$ and temperature $T$ is: $V_{oc}$ (V) $= -0.00177T$ (K) $+ 1.16598$.

## Acknowledgement

This work was performed in the Gansu Supercomputer Center.

## References


[1] Chen X, Zhao Y, Yao R, et al. Impact of lattice volume on the band gap broadening of isovalent S-doped $CuInSe_2$. Journal of Semiconductors, 2008, 29: 1883

[2] Cao J, Qu S, Liu K, et al. Effect of bath temperature on the properties of $CuIn_xGa_{1-x}Se_2$ thin films grown by the electrodeposition technique. Journal of Semiconductors, 2010, 31: 083003

[3] Song J, Li S S, Huang C H, et al. Device modeling and simulation of the performance of $Cu(In_{1-x}, Ga_x)Se_2$ solar cells. Solid-State Electron, 2004, 48: 73

[4] Bouloufa A, Djessas K, Zegadi A. Numerical simulation of $CuIn_xGa_{1-x}Se_2$ solar cells by AMPS-1D. Thin Solid Films, 2007, 515: 6285

[5] Novikov G F, Rabenok E V, Jeng M J, et al. The study of loss kinetics of current carriers in copper-indium-gallium selenide by microwave photoconductivity method. Journal of Renewable Sustainable Energy, 2012, 4: 011604

[6] Ishizuka S, Yamada A, Fons P, et al. Flexible $Cu(In,Ga)Se_2$ solar cells fabricated using alkali-silicate glass thin layers as an alkali source material. Journal Renewable Sustainable Energy, 2009, 1: 013102

[7] Chu S, Majumdar A. Opportunities and challenges for a sustainable energy future. Nature, 2012, 488: 294

[8] Ramanathan K, Contreras M A, Perkins C L, et al. Properties of 19.2% efficiency $ZnO/CdS/CuInGaSe_2$ thin-film solar cells. Progress in Photovoltaics: Research and Applications, 2003, 11: 225

[9] Lin A G, Ding J N, Yuan N Y, et al. Analysis of the $p^+/p$ window layer of thin film solar cells by simulation. Journal of Semiconductors, 2012, 33: 023002

[10] Datta A, Damon-Lacoste J, Cabarrocas P R, et al. Defect states on the surfaces of a p-type c-Si wafer and how they control the performance of a double heterojunction solar cell. Solar Energy Materials and Solar Cells, 2008, 92: 1500

[11] Datta A, Damon-Lacoste J, Nath M, et al. Dominant role of interfaces in solar cells with N-a-Si: H/P-c-Si heterojunction with intrinsic thin layer. Mater Sci Eng B, 2009, 159: 10

[12] Wei S H, Zunger A. Band offsets and optical bowings of chalcopyrites and Zn-based II–VI alloys. J Appl Phys, 1995, 78: 3846

[13] Schroeder D J, Hernandez J L, Rockett A A. Point defects and hole transport in epitaxial $CuIn_{1-x}Ga_xSe_2$. Proceedings of the 11th International Conference on Ternary and Multinary Compounds, 1999: 749

[14] Hanna G, Jasenek A, Rau U, et al. Influence of the Ga-content on the bulk defect densities of $Cu(In,Ga)Se_2$. Thin Solid Films, 2001, 387: 71

[15] Tang F L, Zhu Z X, Xue H T, et al. Optical properties of Al-doped $CuInSe_2$ from the first principle calculation. Physica B, 2012, 407: 4814

[16] Xue H T, Lu W J, Zhu Z X, et al. Al-doped $CuInSe_2$: an *ab initio* study of structural and electronic properties of a photovoltaic material. Advanced Materials Research, 2012, 512–515: 1543

[17] Xue H T, Tang F L, Lu W J, et al. First-principles investigation of structural phase transitions and electronic properties of $CuGaSe_2$ up to 100 GPa. Computational Materials Science, 2013, 67: 21

[18] Wan F C, Tang F L, Zhu Z X, et al. First-principles investigation of the optical properties of $CuIn(S_xSe_{1-x})_2$. Materials Science in Semiconductor Processing, 2013, 16: 1422

[19] Hinuma Y, Oba F, Kumagai Y, et al. Band offsets of $CuInSe_2/CdS$ and $CuInSe_2/ZnS$ (110) interfaces: a hybrid density functional theory study. Phys Rev B, 2013, 88: 035305

[20] Dharmadasa I M. Fermi level pinning and effects on $CuInGaSe_2$-based thin-film solar cells. Semicond Sci Technol, 2009, 24: 055016

[21] Vaynzo Y, Bakulin A A, Gélinas S, et al. Direct observation of photoinduced bound charge-pair states at an organic-Inorganic semiconductor interface. Phys Rev Lett, 2012, 108: 246605

[22] Zhang S B, Wei S H, Zunger A. Stabilization of ternary compounds via ordered arrays of defect pairs. Phys Rev Lett, 1997, 78: 4059

[23] Zhang S B, Wei S H, Zunger A. Defect physics of the $CuInSe_2$ chalcopyrite semiconductor. Phys Rev B, 1998, 57: 9642

[24] Sugiyama M, Nakai R, Nakanishi H, et al. Interface Fermi level pinning in a $Cu/p\text{-}CuGaS_2$ Schottky diode. Journal of Physics and Chemistry of Solids, 2003, 64: 1787

[25] Dharmadasa I M, Bunning J D, Samantilleke A P, et al. Effects of multi-defects at metal/semiconductor interfaces on electrical properties and their influence on stability and life time of thin film solar cells. Solar Energy Materials and Solar Cells, 2005, 86: 373

[26] Dullweber T, Hanna G, Shams-Kolahi W, et al. Study of the effect of gallium grading in $Cu(In, Ga)Se_2$. Thin Solid Films, 2000, 361: 478

[27] Dullweber T, Hanna G, Rau U, et al. A new approach to high-efficiency solar cells by band gap grading in $Cu(In,Ga)Se_2$ chalcopyrite semiconductors. Solar Energy Materials and Solar Cells, 2001, 67: 145

[28] Zhu H, Kalkan A K, Hou J, et al. Application of AMPS-1D for solar cell simulation. AIP Conference Proceedings, 1999, 462: 309

[29] NREL, Solar Spectral Irradiance: Air Mass1.5, http://rredc.nrel.gov/solar/spectra/aml.5/